IEEE Access
Multidisciplinary | Rapid Review | Open Access Journal

Received 16 July 2022, accepted 12 August 2022, date of publication 17 August 2022, date of current version 23 August 2022.

Digital Object Identifier 10.1109/ACCESS.2022.3199360

RESEARCH ARTICLE

New Technique for Improving Modal Filter Performance by Using an Electromagnetic Absorber

YEVGENIY S. ZHECHEV, ALHAJ HASAN ADNAN, AND KONSTANTIN P. MALYGIN
Tomsk State University of Control Systems and Radioelectronics, 634050 Tomsk, Russia

Corresponding author: Yevgeniy S. Zhechev (zhechev75@gmail.com)

This work was supported by the Ministry of Science and Higher Education of the Russian Federation under Project FEWM-2022-0001.

ABSTRACT This paper presents a novel technique for improving modal filter (MF) performance by using an electromagnetic absorber which shows a significant improvement in attenuation of ultra-wideband interference. The authors analyzed the effect of the absorber on the MF performance in suppressing conducted and radiated interferences (in the near and far fields). As an excitation, the authors used an ultra-wideband pulse of 155 ps (at 0.5 level) and then employed N-norms to estimate and characterize the decomposed pulses. It was experimentally demonstrated that the value of N_1 decreased by a factor of 4.31, N_2 – by a factor of 6.52, N_5 – by a factor of 1.87. In terms of radiated interference in the near field, the improvement in attenuation of each norm achieved at least 2.81 times. The analysis of the characteristics in the far field showed that the use of the electromagnetic absorber allows reducing the transmission coefficient on average by 2.25 times at a distance of 1 m.

INDEX TERMS Electromagnetic compatibility and interference, modal filter, ultra-wideband pulse, electromagnetic absorbers, microwave measurement, TEM-cells.

I. INTRODUCTION

Powerful ultra-wideband (UWB) pulses of the nanosecond and sub-nanosecond ranges can penetrate and damage various radioelectronic devices (REDs). Engineers consider conducted interference, induced interference in a system, and radiated interference between systems. To ensure electromagnetic compatibility (EMC) of electronic systems, an electromagnetic interference must be controlled and limited. In comparison with the well-known traditional and constructive techniques that protect circuits against UWB pulses, the recently proposed approach, called modal filtering [1], provides sufficient performance, high power dissipation, small dimensions, and ease in manufacturing. Modal filtering is based on modal distortion of a signal that can occur in a multiconductor transmission line with inhomogeneous dielectric filling thanks to the difference in mode delays [2]. Fig. 1 shows the cross-section and connection diagram of a two-conductor modal filter (MF) to be considered in this study. If the pulse duration is less than the minimum modulus of the difference in mode delays, the interference pulse is decomposed into a sequence of pulses of smaller amplitudes, and their number equals the number of modes.

The main disadvantage of such an MF is a relatively small attenuation of UWB pulses. There are various modifications of MFs that have greater attenuation coefficients [3], [4]. In such structures, the performance could be improved by using additional solutions. For example, quarter-wave resonators, filters with variable wave impedance, or materials with high relative permittivity can be used. However, widely used approaches have several disadvantages (extensive area and mass, small attenuation improvement, high cost, etc.). Therefore, the search and investigation of new techniques to improve the MF performance are relevant, because they can allow expanding the field of application and efficiency of modal-filter-based devices.

In this study, the authors propose a new technique for improving the MF performance. The proposed technique

The associate editor coordinating the review of this manuscript and approving it for publication was Mehmet Alper Uslu.

involves the design of printed circuit boards, in particular, the methods of their assembling. The technical outcome is the reduction of dangerous UWB interference through the combined use of the MF and electromagnetic absorbing material to protect REDs, especially the critical ones.

Usually, such material is widely used to suppress electromagnetic waves [5], [6], [7], [8], [9]. This absorber is used in both civil and military communications devices, aircraft, electronic equipment, etc. [10]. The operating range of the commonly used devices with absorber lies in the high frequency range. This does not allow to consider them as devices to protect power and signal circuits from UWB interference.

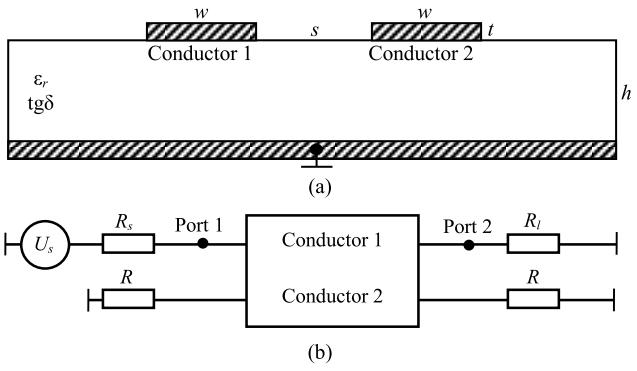

FIGURE 1. (a) Cross-section and (b) connection diagram of the MF.

Significant dielectric and magnetic losses of the electromagnetic absorber, as well as its high values of relative permittivity and permeability, can considerably increase the attenuation of the UWB pulse. Thus, this work is aimed to investigate a new technique that improves the MF performance by using an electromagnetic absorber.

In order to do this, it is necessary to perform a preliminary simulation without taking into account losses and to estimate the effect of the absorber thickness on the MF characteristics. After that, it is necessary to manufacture a prototype of the MF without an absorber and with it, and to carry out measurements in frequency and time domains. To verify the measurement results, it is necessary to perform electrodynamic simulation. Then, it is necessary to feature and analyze the responses to the UWB interference pulse and evaluate the absorber influence on the MF characteristics.

This paper consists of six sections. Section II analyzes the UWB pulse propagation in the MF at different thicknesses of the electromagnetic absorber. Section III describes in detail the MF structure, materials used, simulation methods and measurement techniques. Section IV shows the results in frequency and time domains obtained for conducted and radiated interferences. A comparison that demonstrates the advantages of the proposed technique is given in Section V. Finally, the conclusions are presented in Section VI.

II. UWB PULSE PROPAGATION IN THE MF WITH VARIOUS ABSORBER THICKN ESSES

This Section presents the analysis of UWB pulse propagation in the two-conductor MF with different electromagnetic absorber thickness. Fig. 2 shows the cross-section of the MF with the electromagnetic absorber. In the cross-section, h is the height of the substrate, h_1 is the thickness of the absorber, w is the width of conductors, s is the spacing, t is the conductor thickness.

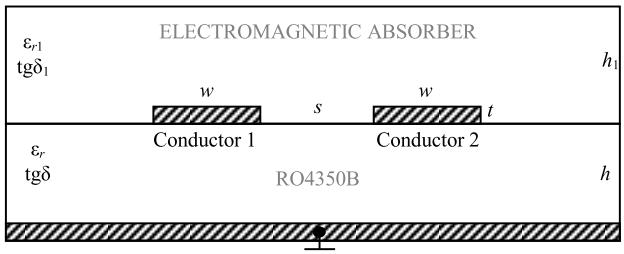

FIGURE 2. Cross-section of the MFs with the electromagnetic absorber.

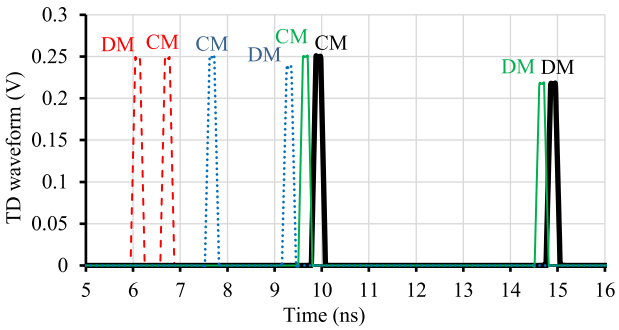

FIGURE 3. TD waveforms on Port 2 obtained during TL analysis for the MF with absorber thicknesses of 0.05 mm (. . .), 0.75 mm (—), and 2 mm (—), as well as the MF without absorber (- - -).

There are two modes propagating in the investigated MF: common mode (CM) and differential mode (DM). In the presence of the absorber, the delays of both modes increase, especially for the differential mode. Since the efficiency of the modal decomposition directly depends on the per-unit-length delays, it is necessary to analyze the influence of the absorber thickness on the UWB pulse propagation. For this purpose, we used transmission lines (TL) analysis for MF without absorber and for MF with absorber. The thickness was varied from 0.05 to 2 mm with a step of 0.05 mm. The MF and the absorber parameters are given in Section III. A trapezoidal signal was used as an exciting UWB pulse with the rise time of 50 ps, and the e.m.f. of 1 V. To easily determine the arrival time of each pulse, the TL analysis was performed without considering losses. Fig. 3 shows the decomposed pulses on Port 2 for the MF with various absorber thicknesses. The relationship between per-unit-length-delays and the absorber thicknesses is shown in Fig. 4.

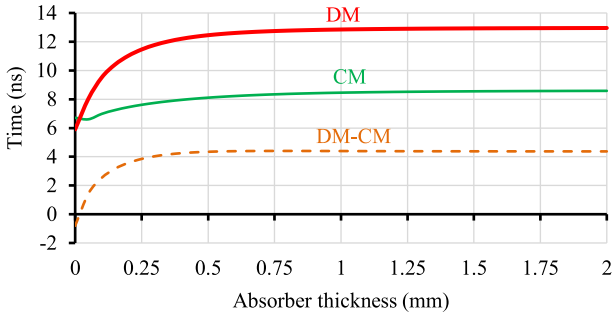

FIGURE 4. Relationship between per-unit-length-delays and the absorber thicknesses.

We can see that the input UWB pulse was decomposed into two pulses of lower amplitudes, and the presence of the absorber significantly increases the per-unit-length delays. Interesting, at first the differential mode was faster than the common mode; however, after adding the absorber the ratio changed. Note that, the thickness of the absorber must be chosen carefully, because, at small h_1, modal decomposition is missing. The figures illustrate that the relationship between the per-unit-length delays and the absorber thicknesses is not linear. Therefore, it is necessary to choose the optimal h_1, which provides a large difference of the per-unit-length delays. Fig. 5 depicts the relative deviation in the difference of per-unit-length delays. We can see that at $h_1 = 0.75$ mm the relative deviation does not exceed 0.1%. Therefore, this value is used in constructing and measuring the prototype.

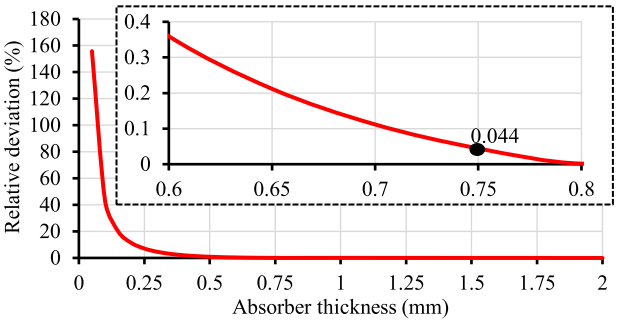

FIGURE 5. Relative deviation of the per-unit-length delay difference.

III. STRUCTURE, MATERIALS, SIMULATION METHODS, AND MEASUREMENT TECHNIQUES

A. STRUCTURE AND MATERIALS

We used ZIPSIL 601 RAM-01 as an electromagnetic absorber. The absorber material is a thin, flexible, elastic, silicone (or fluorosilicon) sheet base, filled with magnetic nano/micro particles of a special shape. In general, it can effectively absorb electromagnetic wave in a frequency range from 100 MHz to 50 GHz. The Eccosorb GDS, BSR, MFS, and CHO-MUTE 9005 absorbers are the closest analogues of such material. At the same time, they have lower insertion losses at high frequencies than ZIPSIL 601 RAM-01.

Fig 3 shows the frequency dependencies of this material parameters up to 6 GHz. Therefore, this absorbing material is widely used to eliminate the parasitic feedbacks in microwave devices; increase the decoupling and noise reduction in microwave microstrip filters; and improve the noise immunity of radar and other microwave devices. As can be seen from Fig. 6, the MF is covered with a thin layer of this material. The RO4350B laminate was used as a substrate material. The device under study consists of two conductors with strong electromagnetic coupling between them. The input of conductor 1 is connected to the UWB pulse source (see Fig. 1). Since the MF is designed to operate in a 50 Ω path, the resistance of the source R_s, load R_l, and resistors R connected to conductor 2 are equal to 50 Ω.

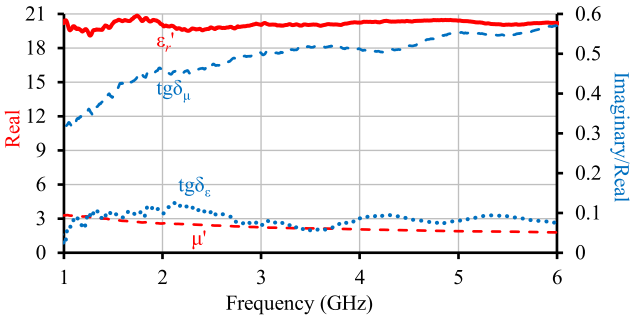

FIGURE 6. Frequency dependences of absorber parameters.

B. MF LAYOUT

The MF layout was made using the standard manufacturing process for double-sided printed circuit boards (PCB). To decompose the UWB interference in the structure, we used the following parameters: $t = 18$ μm, $h = 250$ μm, $w = 500$ μm, $s = 150$ μm, $h_1 = 0.75$ mm. The length l of the MF was 1140 mm. To study the MF in the TEM-cell, the dimensions of the PCB were 98 × 98 mm. Both sides of the PCB were plated with immersion gold to ensure high conductivity and good oxidation resistance. The layer of the electromagnetic absorber was glued to the MF using a liquid absorber with the same characteristics. Fig. 7 shows the manufactured MFs.

To fulfil the decomposition condition with the given MF dimensions, the distances between the adjacent turns were made equal to 3.5 mm. At such distances, the electromagnetic coupling between the turns is low. The coaxial-to-microstrip transitions (Micran PKM2-40) were used to connect the conductor 1 to the measuring equipment. The insertion losses of the transitions did not exceed 0.6 dB in the frequency range from 0 to 40 GHz. To reduce reflections from the structure, SMD resistors (size 0805) were connected to conductor 2.

C. MEASUREMENT TECHNIQUES

Fig. 8 shows the experimental setup used to analyze the frequency characteristics of the MFs. The MF under investigation was located inside the TEM-cell [11] to exclude the

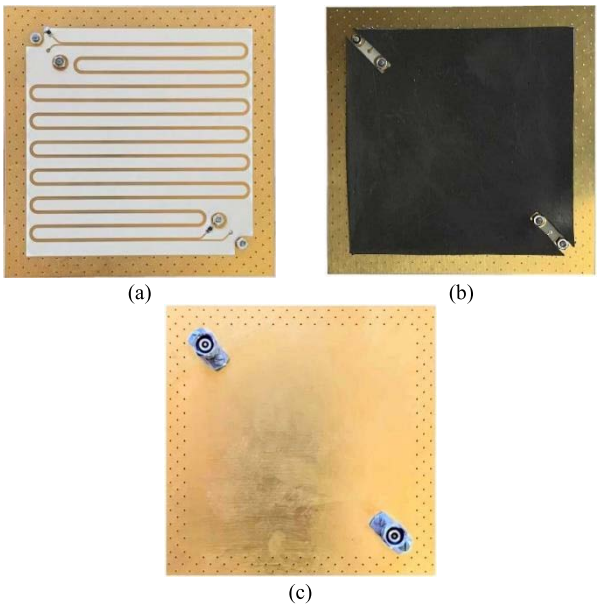

FIGURE 7. PCB layout: top sides for the MFs (a) without and (b) with absorber, and (c) bottom side for both structures.

radiated interference from the outside. The TEM-cell with the MF was connected to the 2-port vector network analyzer (VNA) using high-frequency cables. The Panorama P4226 (Micran) with an operating frequency range from 10 MHz to 26.5 GHz was used as the VNA. The measuring equipment was calibrated in the operating frequency range of the TEM-cell from 10 MHz to 5.2 GHz. To consider the orientation of the electromagnetic field in the TEM-cell, the PCB was rotated in 90 degree increments. We analyzed the worst characteristics for the MFs with and without the absorber.

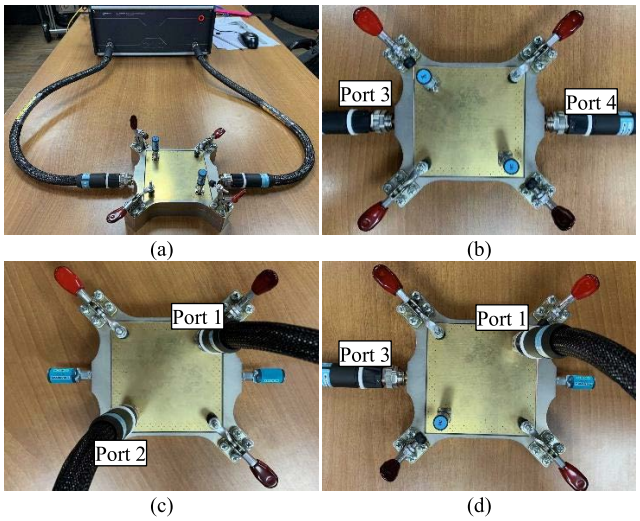

FIGURE 8. Measurement setup to analyze the MFs in the frequency domain: (a) general view, (b) setup for analyzing TEM-cell, (c) conducted and (d) radiated characteristics.

To analyze the responses in the time domain, we used Advanced Design System where the obtained S-parameters were imported (Fig. 9). A Gaussian pulse with a total duration of 680 ps and an e.m.f. amplitude of 1 V was excited as a UWB interference. This excitation was selected because the majority of its spectrum (about 96%) is in the frequency range under consideration. Such UWB interference is in full accordance with the description from the EMC standard [12]. Fig. 10 shows the time domain (TD) waveform of the UWB pulse and its voltage spectral density S.

New RED's have various complex types and constructions. In some cases, the distance between small-size subsystems in one system case may be larger than the wavelength of the emitted radiation if the system is operating at high frequencies. Since an MF is a protection device used to ensure EMC of the final product, its frequency characteristics should be evaluated in the far field.

FIGURE 9. Circuit for simulating conducted and radiated emissions in the ADS.

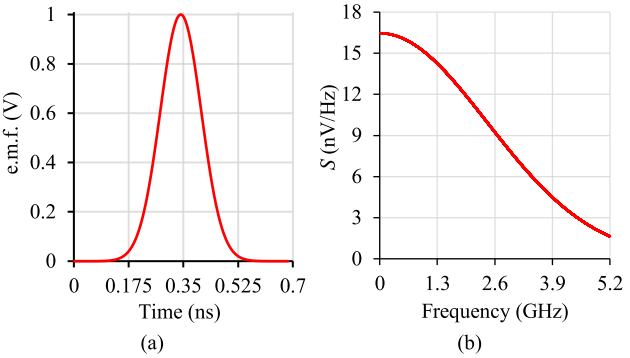

FIGURE 10. (a) The e.m.f. waveform of the UWB pulse interference and its (b) voltage spectral density.

To study the features of the MF with the absorber in the far field, an experiment shown in Fig. 11 was carried out. The coaxial-to-microstrip transitions were used to connect Port 1 to the measuring equipment (PLANAR C1220 0.1 MHz–20 GHz). Port 2 was connected to a 50 Ω load. The VNA was connected to the ZIPSIL ARB-133 horn antenna. The antenna is designed to solve a wide range of technical problems related to measuring RF and microwave electromagnetic waves in a wide frequency range. The antenna has a wide operating frequency range from 1 to 33 GHz, a high gain up to 18 dB, a low VSWR value, and a low level of the rear lobes of the radiation pattern. First, the system was calibrated in the presence of the MF without the absorber. Then, the absorber was placed on the MF, and the transmission coefficient of the system was obtained. This gave the attenuation of the transmission coefficient when using the absorber. The antenna was located at 1 m distance above the MF at 0° vertically.

FIGURE 11. Measurement setup to analyze radiated characteristics of the MF in the far field.

D. SIMULATION METHODS

The finite difference time domain (FDTD) method implemented in the EMPro software was used for simulating the MF. This method solves the Maxwell equations in the time domain and fully describes the MFs under investigation. As a result, complex and frequency-dependent electrical parameters of the structure were obtained. During the simulation, we took into account the dielectric and absorber losses, as well as the finite conductivity of the conductors [13].

To analyze the MF characteristics in the near-field, we simulated the regular part of the TEM-cell, which was used in the measurements. The simulation was performed in the frequency range from 10 MHz to 5.2 GHz. The geometrical and electrical parameters of the TEM-cell are presented in [11]. The MF under study was located in the upper part of the case at a distance of 15 mm from the central conductor. In this simulation, the perfect electrical conductor was used as a material of the outer boundaries for all directions. The RO4350B laminate with relative dielectric permittivity (ε_r) of 3.66 and tangent of loss angle (tgδ) of 0.0037 was used as a dielectric substrate (the parameters are presented for the frequency of 10 GHz). The conductive layers were made of copper with a conductivity of $5.96{\cdot}10^7$ S/m.

To analyze the MF in the far field using the FDTD method, we used a broadband pulse with a signal amplitude of 1 V. All terminations were loaded with 50 Ω resistances. The MF was simulated using a mesh with basic cell size equal to the 1/60 of the wavelength of the maximum frequency (from 3 to 6 GHz) until convergence. The electric field strength was calculated at a distance of 1 m, and the far field geometry sensor was built using spherical coordinate system when angles θ and φ were changed in general, from 0° to 180° in 1° increments.

E. UWB PULSE CHARACTERIZATION

The UWB pulse is dangerous for electronic equipment for many reasons. For example, its large amplitude can lead to electrical breakdown, fast rise time – to spark formation, average effective voltage value – to component burnout, etc. We used the N-norms [14] which were applied by the authors in similar studies to comprehensively evaluate the hazards of input and decomposed pulses [15], and to compare the suppression efficiency of the absorber. Table 1 shows the names, formulas, and descriptions of each norm, reproduced from [16], [17].

TABLE 1. N-norms descriptions and applications.

Norm	Name	Equation	Application
N_1	Peak value (absolute)	$\lvert U(t)\rvert_{\max}$	Circuit upset / electric breakdown / arc-over effects
N_2	Peak derivative (absolute)	$\left\lvert \frac{dU(t)}{dt} \right\rvert_{\max}$	Component arcing / circuit upset
N_3	Peak pulse (absolute)	$\left\lvert \int_0^t U(t)\,dt \right\rvert_{\max}$	Dielectric puncture (if U denotes E field)
N_4	Rectified general pulse	$\int_0^{\infty} \lvert U(t)\rvert dt$	Equipment damage
N_5	Square root of the action integral	$\left\{ \int_0^{\infty} \lvert U(t)\rvert^2\, dt \right\}^{\frac{1}{2}}$	Component burnout

*$U(t)$ is the TD waveform of the UWB pulse (Port 1 for input excitation, Port 2 for decomposed pulses, Port 3 for induced voltages in the near field).

IV. MEASUREMENT AND SIMULATION RESULTS

A. STRUCTURE AND MATERIALS

As the MF can act as a low pass filter, it is important to investigate the influence of using the absorber on the basic conducted characteristics of MF which are the signal decomposition and the cut-off (f_c) and resonance (f_r) frequencies of the transmission coefficient. To do this, the MF with the absorber and without it was simulated in the frequency and time domains. The obtained results were compared to the measured ones as the setup c from Fig. 8. The compared frequency dependent $|S_{21}|$ and TD waveforms on Port 2 are presented in Fig. 12.

Table 2 summarizes the obtained characteristics, and Table 3 shows the calculated N-norms for the decomposed pulses (input excitation was obtained without MF on the ideal load). The use of the absorber significantly increased the insertion loss in the stopband. Thus, bandwidth frequency f_c decreased from 335 to 60 MHz (obtained for measurements). The shift of f_r by 660 MHz is caused by the increased per-unit-length delays of the modes because of the absorber.

The time characteristics show that the input UWB pulse is decomposed into two pulses of smaller amplitudes. Application of the absorber made it possible to significantly reduce the amplitude of the decomposed pulses and increase the per-unit-length delays. As a result, the MF with an absorber can decompose the UWB pulse of longer duration.

Table 3 shows that the MF attenuates the UWB pulse. Application of the absorber allows for the significant increase in the total attenuation. It was experimentally demonstrated

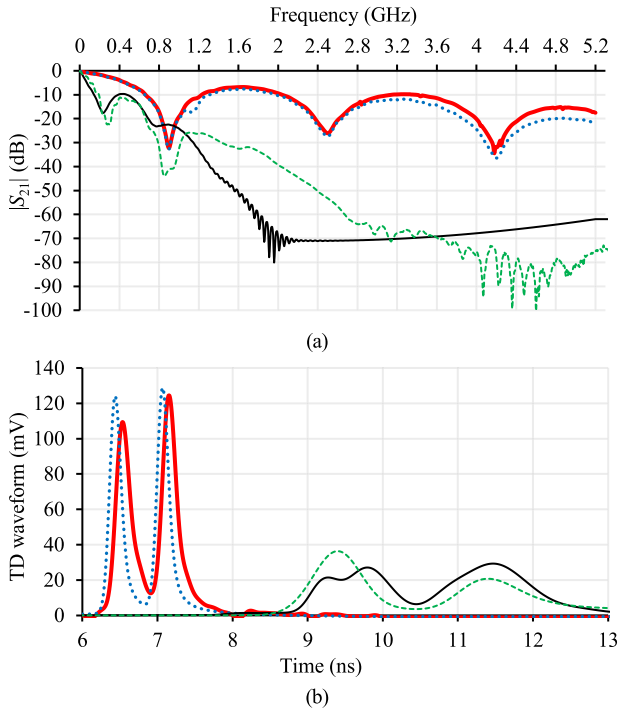

FIGURE 12. (a) Frequency dependent $|S_{21}|$ and (b) TD waveforms on Port 2 obtained during measurements (—) and simulation (•••) of the MF without the absorber and measurements (—) and simulation (- - -) of the MF with the absorber.

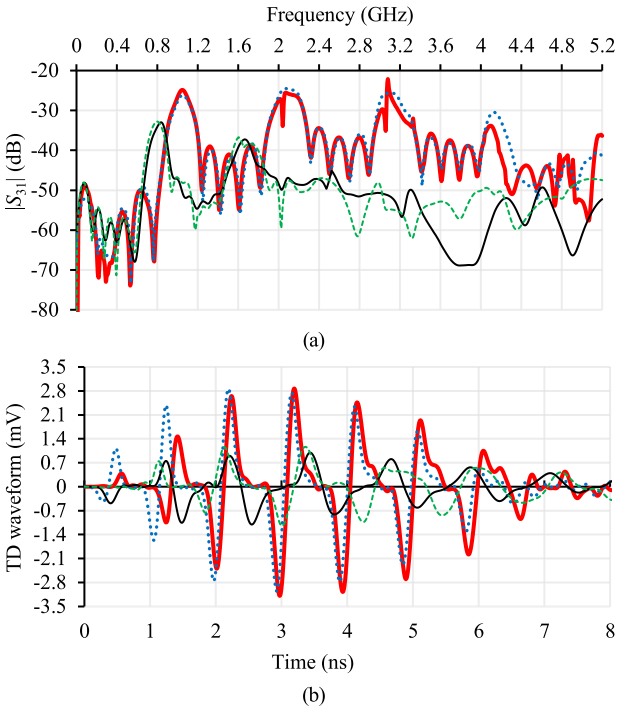

FIGURE 13. (a) Frequency dependent $|S_{31}|$ and (b) TD waveforms on Port 3 obtained during measurements (—) and simulation (•••) of the MF without the absorber and measurements (—) and simulation (- - -) of the MF with the absorber.

TABLE 2. MF characteristics on Port 2.

	f_c, MHz	f_r, MHz	U_1, mV	U_2, mV
MF without absorber (Measurement)	335	900	106	125
MF without absorber (Simulation)	325	895	123	129
MF with absorber (Measurement)	60	240	27	29
MF with absorber (Simulation)	75	280	36	21

that the value of N_1 decreased by a factor of 4.31, N_2 – by a factor of 6.52, N_5 – by a factor of 1.87. It can be seen that the MF with the absorber strongly attenuates the input impact: N_1 by 17.2 times, N_2 by 70 times, N_5 by 4.6 times. As a result of the complex influence on the UWB pulse, the probability of occurrence of various types of failures decreases.

TABLE 3. Calculated *N*-norms of the decomposed pulses on Port 2.

	N_1	N_2	N_3	N_4	N_5
Input Excitation	0.5	$4.61{\cdot}10^{9}$	$82{\cdot}10^{-12}$	$82{\cdot}10^{-12}$	$5.39{\cdot}10^{-6}$
MF without absorber (Measurement)	0.125	$0.43{\cdot}10^{9}$	$65{\cdot}10^{-12}$	$66{\cdot}10^{-12}$	$2.19{\cdot}10^{-6}$
MF without absorber (Simulation)	0.129	$0.53{\cdot}10^{9}$	$57{\cdot}10^{-12}$	$58{\cdot}10^{-12}$	$2.12{\cdot}10^{-6}$
MF with absorber (Measurement)	0.029	$6.59{\cdot}10^{7}$	$64{\cdot}10^{-12}$	$65{\cdot}10^{-12}$	$1.17{\cdot}10^{-6}$
MF with absorber (Simulation)	0.036	$6.71{\cdot}10^{7}$	$63{\cdot}10^{-12}$	$62{\cdot}10^{-12}$	$1.08{\cdot}10^{-6}$

B. RADIATED EMISSIONS

The MF has an advantage since it may be manufactured with small dimensions and low mass which expanding the scope of its application especially in PCB designing. Therefore, it is important to investigate its radiated characteristics which is equally significant as the conducted ones. Thus, to estimate the level of the radiated emissions from the MF with the absorber and without it, the MF was modeled in the frequency and time domains. The results obtained in the near field were compared to those measured as the setup d from Fig. 8, and the results obtained in the far field were compared to measured as in Fig. 11 ones. Fig. 13 shows frequency dependent $|S_{31}|$ and TD waveforms on Port 3 obtained during measurements and simulation. Table 4 summarizes the obtained characteristics, and Table 5 shows the calculated N-norms for induced voltage waveforms.

The frequency characteristics show that the use of the absorber allowed reducing the average value of $|S_{31}|$. Thus, the attenuation of 10.54 dB was achieved in measurements, and 9.84 dB in the simulation. At the same time the attenuation of the maximum value of $|S_{31}|$ was obtained at 10.89 dB during the measurements, and 8.29 dB during the simulation. In terms of time characteristics, we can see that the maximum amplitude U_{max} decreased by 2.58 times, and the minimum U_{min} decreased by 2.9 times. From the point of view of N-norms, we can see that the use of the absorber allowed a significant reduction of each of the norms. The smallest attenuation was 2.81 times for N_4 obtained during

TABLE 4. MF characteristics on Port 3.

	$\|S_{31}\|_{aver}$, dB	$\|S_{31}\|_{max}$, dB	U_{max}, mV	U_{min}, mV
MF without absorber (Measurement)	-42.55	-22.12	2.87	-3.19
MF without absorber (Simulation)	-41.51	-24.51	2.86	-3.04
MF with absorber (Measurement)	-53.09	-33.01	1.11	-1.15
MF with absorber (Simulation)	-51.35	-32.8	0.95	-1.1

TABLE 5. Calculated *N*-norms of the decomposed pulses on Port 2.

	N_1	N_2	N_3	N_4	N_5
Input Excitation	0.5	$4.61\cdot10^{9}$	$82\cdot10^{-12}$	$82\cdot10^{-12}$	$5.39\cdot10^{-6}$
MF without absorber (Measurement)	$3.2\cdot10^{-3}$	$41\cdot10^{6}$	$46\cdot10^{-15}$	$5.43\cdot10^{-12}$	$92\cdot10^{-9}$
MF without absorber (Simulation)	$3\cdot10^{-3}$	$19\cdot10^{6}$	$52\cdot10^{-15}$	$4.98\cdot10^{-12}$	$88\cdot10^{-9}$
MF with absorber (Measurement)	$0.98\cdot10^{-3}$	$9.2\cdot10^{6}$	$7.74\cdot10^{-15}$	$1.93\cdot10^{-12}$	$26.4\cdot10^{-9}$
MF with absorber (Simulation)	$0.99\cdot10^{-3}$	$12\cdot10^{6}$	$11.5\cdot10^{-15}$	$2.56\cdot10^{-12}$	$37.1\cdot10^{-9}$

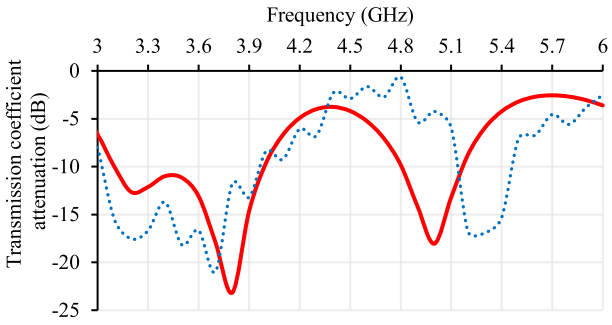

FIGURE 14. The measured (—) and calculated (•••) attenuation of the MF transmission coefficient in the far field when using the absorber.

the measurements. As in the case of conducted interference, we can conclude that the use of an absorber can reduce the probabilities of failure.

Fig. 14 shows the calculated and the measured attenuation of the transmission coefficient when using the absorber, obtained in the far field at a distance of 1 m from the MF. The results have a similar behavior in the studied frequency range. Table 6 shows the obtained maximum, minimum, and average attenuation value. The calculated average attenuation value is about 9.3 dB and the measured one – 8.7 dB. Since the transmission coefficient is attenuated, one can say that the radiated emmision from the MF will be reduced.

V. COMPARATIVE ANALYSIS

To evaluate the efficiency of the proposed technique for improving MF performance, we compared it with five other methods. Table 7 presents their advantages and disadvantages. The proposed method of improving the MF performance by adding an absorber layer according to the total score of the selected criteria shows higher results than others. The main disadvantage of techniques based on adding quarter-wave resonators, introducing asymmetry in the cross section for the appearance of additional pulses, and the method of cascading the TLs is small difference between the per-unit-length delays of modes. In addition, implementing quarter-wave resonators requires more time to design, optimize, and place them in the production stage of the MF. The disadvantage of meander lines is small attenuation of UWB interference. To reduce its amplitude at the output of the meander line, a large line length is required, which entails an increase in size and makes it difficult to integrate into an actual device. Techniques based on the addition of passive conductors and cascade connection also have this disadvantage. However, their main advantages are ease of manufacture and lower cost. The proposed technique also has a disadvantage that is not the case with most other methods. The properties of absorbing material complicate the MF implementation. However, with the appropriate design of an MF with an absorber, it is possible to achieve significant attenuation of the UWB interference without increasing PCB size.

TABLE 6. The attenuation of the transmission coefficient in the far field.

	Simulation	Measurement
Minimum	20.96 dB	23.16 dB
Maximum	0.65 dB	2.55 dB
Average	9.28 dB	8.70 dB
Average absolute deviation	$(\|X_2-X_1\|/\|X_2+X_1\|)\% = \pm29\ \%$*	

*X_1 is the first comparable value, X_2 is the second comparable value.

TABLE 7. Comparing various techniques for improving MF performance.

Technique	UWB interference suppression	Differences of per-unit-length delays	Dimensions and weight	Manufacturability
Proposed technique	Significant	Significant	Average	Difficult
Quarter-wave resonators [4]	Average	Insignificant	Large	Difficult
Meander line tracing [18]	Insignificant	Average	Small	Easy
Additional pulses [3], [19]	Average	Insignificant	Average	Easy
Additional passive conductors [19]	Average	Average	Small	Average
Cascade connection [21]	Significant	Insignificant	Small	Average

VI. CONCLUSION

The modified MF based on the proposed technique demonstrated apparent advantages compared with classical MFs. The authors presented the description and analysis results with high-frequency measurements. It was experimentally determined that by using the technique the value of N_1

decreased by a factor of 4.31, N_2 – by a factor of 6.52, N_5 – by a factor of 1.87. In terms of radiated interference in the near field, the improvement in attenuation of each norm was at least 2.81 times. The analysis of the characteristics in the far field showed that the use of the absorber allowed reducing the transmission coefficient on average by 9 dB. The obtained results demonstrate the possibility of using the electromagnetic absorbing material to enhance the performance of the MF-based protection device. Moreover, the presence of the absorber does not have a negative impact on the modal distortion of the signal.

REFERENCES

[1] T. R. Gazizov and A. M. Zabolotsky, "New approach to EMC protection," in *Proc. 18th Int. Zurich Symp. Electromagn. Compat.*, Sep. 2007, pp. 273–276, doi: 10.1109/EMCZUR.2007.4388248.

[2] A. T. Gazizov, A. M. Zabolotsky, and T. R. Gazizov, "UWB pulse decomposition in simple printed structures," *IEEE Trans. Electromagn. Compat.*, vol. 58, no. 4, pp. 1136–1142, Aug. 2016, doi: 10.1109/TEMC.2016.2548783.

[3] M. A. Samoylichenko, Y. S. Zhechev, V. P. Kosteletskii, and T. R. Gazizov, "Electrical characteristics of a modal filter with a passive conductor in the reference plane cutout," *IEEE Trans. Electromagn. Compat.*, vol. 63, no. 2, pp. 435–442, Apr. 2021, doi: 10.1109/TEMC.2020.3011407.

[4] Y. Zhechev and A. Zabolotsky, "The use of quarter-wave resonators to improve modal filters performance," in *Proc. IEEE 22nd Int. Conf. Young Professionals Electron Devices Mater. (EDM)*, Jun. 2021, pp. 204–207, doi: 10.1109/EDM52169.2021.9507692.

[5] T. Tobana, T. Sasamori, K. Abe, Q. Chen, and K. Sawaya, "Suppression effect of the emission from printed circuit board using magnetic absorber located along microstrip line," in *Proc. IEEE Int. Symp. Electromagn. Compat. (EMC)*, May 2003, pp. 1248–1251, doi: 10.1109/ICSMC2.2003.1429145.

[6] X. Jiao, P. Maheshwari, V. Khikevich, P. Dixon, Y. Arien, A. Bhobe, J. Li, X. Li, D. Pommerenke, J. Drewniak, H. Kajbaf, and J. Min, "EMI mitigation with lossy material at 10 GHz," in *Proc. IEEE Int. Symp. Electromagn. Compat. (EMC)*, Aug. 2014, pp. 150–154, doi: 10.1109/ISEMC.2014.6898960.

[7] Q. Liu, X. Jiao, J. Li, V. Khilkevich, J. Drewniak, P. Dixon, and Y. Arien, "Modeling absorbing materials for EMI mitigation," in *Proc. IEEE Int. Symp. Electromagn. Compat. (EMC)*, Aug. 2015, pp. 1548–1552, doi: 10.1109/ISEMC.2015.7256405.

[8] M. A. Khorrami, P. Dixon, Y. Arien, and J. Song, "Effective power delivery filtering of mixed-signal systems with negligible radiated emission," *IEEE Electromagn. Compat. Mag.*, vol. 5, no. 4, pp. 128–132, 4th Quart., 2016, doi: 10.1109/MEMC.2016.7866251.

[9] P. Zuo, T. Li, M. Wang, H. Zheng, and E.-P. Li, "Miniaturized polarization insensitive metamaterial absorber applied on EMI suppression," *IEEE Access*, vol. 8, pp. 6583–6590, 2020, doi: 10.1109/ACCESS.2019.2957308.

[10] M. M. Tirkey and N. Gupta, "The quest for perfect electromagnetic absorber: A review," *Int. J. Microw. Wireless Technol.*, vol. 11, no. 2, pp. 151–167, Mar. 2019, doi: 10.1017/S1759078718001472.

[11] A. V. Demakov and M. E. Komnatnov, "TEM cell for testing low-profile integrated circuits for EMC," in *Proc. 21st Int. Conf. Young Spec. Micro/Nanotechnol. Electron Devices (EDM)*, Jun. 2020, pp. 154–158, doi: 10.1109/EDM49804.2020.9153508.

[12] *Electromagnetic Compatibility (EMC)—Part 1-5: High Power Electromagnetic (HPEM) Effects on Civil Systems*," document IEC. 61000-1-5, 2004.

[13] C. Svensson and G. H. Dermer, "Time domain modeling of lossy interconnects," *IEEE Trans. Adv. Packag.*, vol. 24, no. 2, pp. 191–196, May 2001, doi: 10.1109/6040.928754.

[14] E. Baum, "Norms and eigenvector norms," *Math. Notes*, vol. 63, Nov. 1979, pp. 1–42.

[15] Y. S. Zhechev, A. V. Zhecheva, A. A. Kvasnikov, and A. M. Zabolotsky, "Using N-norms for analyzing symmetric protective electrical circuits with triple modal reservation," *Symmetry*, vol. 13, no. 12, p. 2390, Dec. 2021, doi: 10.3390/sym13122390.

[16] D. Giri, *High-Power Electromagnetic Radiators: Nonlethal Weapons and Other Applications*. Cambridge, MA, USA: Harvard University Press, 2004.

[17] *Electromagnetic Compatibility (EMC)—Part 4-33: Testing and Measurement Techniques—Measurement Methods for High-Power Transient Parameters*, document IEC. 61000-4-33, 2005.

[18] R. S. Surovtsev, A. V. Nosov, and T. R. Gazizov, "Comparison of time responses of a meander line turn to ultrashort pulse excitation," *IEEE Trans. Electromagn. Compat.*, early access, Apr. 26, 2022, doi: 10.1109/TEMC.2022.3162640.

[19] A. O. Belousov, E. V. Chernikova, M. A. Samoylichenko, A. V. Medvedev, A. V. Nosov, T. R. Gazizov, and A. M. Zabolotsky, "From symmetry to asymmetry: The use of additional pulses to improve protection against ultrashort pulses based on modal filtration," *Symmetry*, vol. 12, no. 7, p. 1117, 2020, doi: 10.3390/sym12071117.

[20] A. O. Belousov, I. V. Romanchenko, and T. R. Gazizov, "The use of multiconductor strip structures for splitting an ultrashort pulse in its generation systems," *J. Phys., Conf.*, vol. 1399, no. 2, Dec. 2019, Art. no. 022049, doi: 10.1088/1742-6596/1399/2/022049.

[21] M. A. Samoylichenko and A. M. Zabolotsky, "Simulation the time response to ultra-short pulse excitation of two cascaded modal filters with a passive conductor in the reference plane," *J. Phys., Conf.*, vol. 1611, no. 1, pp. 1–5, 2020, doi: 10.1088/1742-6596/1611/1/012030.

YEVGENIY S. ZHECHEV was born in Almaty, Kazakhstan, in 1994. He received the B.Sc. and M.Sc. degrees in infocommunication technologies and communication systems from the Tomsk State University of Control Systems and Radioelectronics (TUSUR), Tomsk, Russia, in 2016 and 2018, respectively, where he is currently pursuing the Ph.D. degree in electromagnetic compatibility of radioelectronic devices.

He has over five years of experience with electromagnetic compatibility issues. He has authored or coauthored over 50 refereed publications. His current research interests include time-domain electromagnetic modeling techniques, electromagnetic compatibility, microwave transmission lines, and power protective devices.

ALHAJ HASAN ADNAN was born in Syria, in 1990. He received the B.S. degree in information and communication technologies from the University of Tartous, Syria, in 2016, and the M.S. degree in radio-technical engineering from Tambov State Technical University, Tambov, Russia, in 2019. He is currently pursuing the Ph.D. degree in electromagnetic compatibility of radioelectronic devices with TUSUR.

He has over three years of experience with electromagnetic compatibility issues. He has authored or coauthored over 25 refereed publications. His current research interests include electromagnetic compatibility, high-speed interconnects and antennas computer modeling, and numerical algorithms.

KONSTANTIN P. MALYGIN was born in Gusinoozersk, Russia, in 1997. He received the B.Sc. degree in service and the M.Sc. degree in infocommunication technologies and communication systems from TUSUR, Tomsk, Russia, in 2018 and 2020, respectively, where he is currently pursuing the Ph.D. degree in electromagnetic compatibility of radioelectronic devices.

He has over two years of experience with electromagnetic compatibility issues. His current research interests include time-domain electromagnetic modeling techniques, electromagnetic compatibility, microstrip lines, meander lines, and optimization.